Control Engineering Practice 82 (2019) 72–85

Contents lists available at ScienceDirect

Control Engineering Practice

journal homepage: www.elsevier.com/locate/conengprac

Current control based power management strategy for distributed power generation system

Doğan Çelik, Mehmet Emin Meral *

Department of Electrical and Electronics Engineering, Van Yuzuncu Yıl University, Van, Turkey

ARTICLE INFO

Keywords:
Current control
Positive–negative sequences
Distributed generation
Power management
Reference current generator
Oscillations

ABSTRACT

The integration of renewable energy sources (RES) based distributed generation (DG) systems into electric grid has many challenges such as synchronization, control, power management (PM) and power quality problems. This paper proposes a references current generator (RCG) based PM strategy to control three phase inverter and manage power flow among the DG energy sources, electric grid and load demand under balanced and unbalanced grid conditions. The amplitudes of active and reactive power oscillations are also eliminated and controlled through only one flexible control parameter (FCP) under grid faults and harmonic distortions. Compared with previous similar studies, one of the important contributions is capable to inject maximum active power and minimum reactive power into electric grid and load at inverter power capacity under grid faults Another contribution is to extract the positive and negative sequence (PNS) voltage and current components with the improved fast and robust dual adaptive filters based phase locked loop (DAF-PLL). Fractional order proportional integral (FOPI) is selected as an attractive solution for AC current regulation to exhibit fast transient response and to achieve zero steady-state errors as compared with conventional current regulation controllers in synchronous or stationary frames.

1. Introduction

The conventional power systems have many problems such as using fossil fuels which result in very high costs; greenhouse gas emissions and pollution are exhaustible and limited in supply and have long transmission lines, large amount of technical and nontechnical losses (Amin & Wollenberg, 2005; Wu, Hu, Teng, et al., 2017). The modern power generation technologies have encouraged changes in the power system structure (Cau, Cocco, Petrollese, et al., 2014; Divshali & Choi, 2016). In order to overcome these limitations and problems, renewable energy sources (RES) based distributed generation (DG) power systems can cope with environmental issues, energy crises and remove the drawback of a single RES by taking the best possible use of each individual energy source. The main drawbacks of RES, such as wind turbines (WT) and photovoltaic cell (PV) have discontinuity for energy generation (Cau et al., 2014; Kamali, Rahim, & Mokhlis, 2014). To avoid overloading power converter, current controller limit power that fuel cell (FC) unit can supply power to grid. However, power limitation result in slow dynamic response the FC unit (Das, Padmanaban, Venkitusamy, et al., 2017). The various controllers such as model predictive controller and sliding mode controller can be used to deal with the slower dynamics of the FC. In particular, the purpose of control algorithms based power management (PM) strategy in DG power systems guarantees continuity of energy, optimum use of power capability of inverter and maximum utilization of renewable sources in all conditions. Key issues for grid connected DG power systems consist of control and PM strategy (Olatomiwa, Mekhilef, Ismail, et al., 2016). The control algorithm based PM strategy is also significantly important to supply maximum active power and minimum reactive power delivery capability under balanced and unbalanced conditions according to power demand.

Advanced control algorithms based PM strategy has been reported to achieve a balance active power in recent studies. Bayrak, Bayrak, Ozdemir, et al. (2016) focuses on low cost power management for hybrid power plant. Predictive control based PM is designed to coordinate power flow between various energy sources (Brka, Kothapalli, & Al-Abdeli, 2015). An energy management optimization is proposed to overcome power quality problems for power units and batteries (Li, Wang, Chen, et al., 2017; Panda & Patnaik, 2017). Coordinated control strategy is designed for PM of solid oxide fuel cell (FC) based microgrid. Power balance principle is used in coordinated control strategy of grid connected inverter systems (Sun, Wu, Xue, et al., 2018). Other control method is that positive and negative sequence (PNS) control based on the sliding mode control and Lyapunov function theory are designed for hybrid AC/DC WT/PV/FC microgrid (Baghaee, Mirsalim, Gharehpetian, et al., 2017). Dash, Samanta, and Ganesan (2016) and Yumurtaci (2013) have proposed two PM strategy to control standalone and grid connected hybrid system. The impact of weather conditions

* Corresponding author.
E-mail addresses: dogancelik@yyu.edu.tr (D. Çelik), emeral@yyu.edu.tr (M.E. Meral).

https://doi.org/10.1016/j.conengprac.2018.09.025
Received 13 May 2018; Received in revised form 25 July 2018; Accepted 25 September 2018
Available online 11 October 2018
0967-0661/

on WT and PV systems are analyzed and investigated. However, the impact of grid faults on control of inverter interfaced DG system and injected active–reactive power are not considered in these studies. The grid faults have been shown to be one of the greatest challenges for conventional inverter control to provide maximum power capability at inverter capacity. In order to ensure balanced current, constant active power and reduce active and reactive power oscillations, some researchers have investigated positive and negative sequence (PNS) based reference current generators (RCG) (Kabiri, Holmes, & McGrath, 2016; Wang, Duarte, & Hendrix, 2010). Active and reactive powers and their oscillations are independently controlled with two flexible control parameters (FCP) in stationary reference frame (STRF) by Wang, Duarte, and Hendrix (2011). Karimi-Ghartemani, Khajehoddin, Piya, et al. (2016) and Piya, Ebrahimi, Karimi-Ghartemani, et al. (2018) have been proposed a universal controller that achieve robust against uncertainties and change of the grid parameters. Embedded synchronization into controller provides agile and smooth responses without stability issues. Other interesting power control method is reported that a new vector transformation based instantaneous p-q power control is enhanced by Montanari and Gole (2017). However, the controllable of active–reactive power oscillations is difficult because of using two adjustable control parameters. Sosa, Castilla, Miret, et al. (2016) proposes maximum power capability of inverter and avoid only active power oscillation with using two FCP. Maximum power deliver allowed by inverter and active power oscillations are discussed under various scenarios by Lopez, De Vicuna, Miret, et al. (2018). The PM strategy and power flow between DG energy sources, grid and load demand are not taken into consideration in these studies. The PNS components are also obtained from slow (longer than two cycles) conventional sequence extractors to obtain the RCG.

The PNS components are significantly essential module to obtain the RCG under unbalanced conditions. Various researchers have been investigated PNS extractors to generate reference current in the literature. Dual second-order generalized integrator (DSOGI) (Sun, Chen, Wang, et al., 2016; Zhang, Rocabert, Candela, et al., 2017), delay signal cancelation based PLL (DSC-PLL) (Jin, Li, Li, et al., 2017; Meral, 2012), double synchronous reference (DSRF) or decoupled double synchronous reference (DDSRF) (Ali, Christofides, Hadjidemetriou, et al., 2017; Reyes, Rodriguez, Vazquez, et al., 2012; Rodriguez, Pou, Bergas and et al., 2007), moving average filter (MAF) (Mirhosseini, Pou, & Karanayil) and multivariable filter (MVF) (Meral & Çelik, 2018a; Wang et al., 2010) are presented for separation of PNS components in STRF or synchronous reference frame (SRF) under unbalanced conditions. Recently, another approaches have been emerged, multi complex coefficient filter (MCCF)-PLL (Guo, Wu, & Chen, 2011) and third order sinusoidal integrator (TOSSI) (Chilipi, Al Sayari, Al Hosani, et al., 2016, 2018). Two PNS extractors separate fast and more robust PNS components. However, the impact of voltage harmonics, including many sub-modules, dynamic response and computational burden still seem problems for signal processing in abovementioned PNS extractors.

This paper proposes a current control method based improved PM strategy to manage active power flow among DG units (PV, FC and WT), electric grid and various loads under balanced and unbalanced conditions. In particular, the PM strategy is not discussed under grid faults and discontinuity of energy sources in previous similar studies. Various PM scenarios have been performed to manage active power flow among DG units. This paper provides some advantages in fourfold: (1) in order to generate reference current, the PNS voltage–current components are separated by improved DAF-PLL, which provides fast dynamic response and is less affected by harmonic distortions and grid faults. Its performance is examined and compared with existing PNS extractors, (2) the proposed control algorithm based PM strategy increase the inverter power capability by injecting the maximum active current and minimum reactive current under grid faults, (3) the current tracking errors are minimized by fractional order proportional integral (FOPI), which exhibits fast dynamic response in compared with conventional current regulation controllers in SRF or STRF and (4) active–reactive power oscillations are regulated and controlled by only one FCP. Performance comparison of proposed solution is comprehensively tested and reviewed with some previous studies.

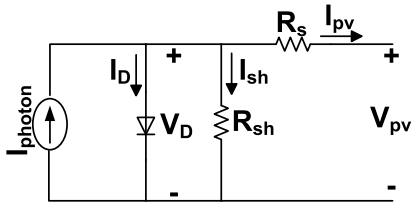

Fig. 1. Equivalent circuit for a PV cell.

The outline of the paper is structured as follows. Following introduction, Section 2 briefly describes the DG energy sources based on mathematical computation. The performance comparisons of improved DAF-PLL based sequence extractor is presented and analyzed with existing PNS extractors in Section 3. Section 4 formulates problem statement for proposed solution. In Section 5, proposed RCG based control strategy is introduced for maximum power deliver and PM strategy. The implementation of proposed system is verified, compared and tested under various cases in Section 6. Section 7 summarized the conclusion derived from this study. All nomenclatures are given in Table 1.

2. Distributed generation (DG) energy sources

The DG power system consists of combination of PV cell, FC and WT at common DC bus. All local current/power controllers for PV cell, FC and WT are designed to control the power flow among the DG system, load demand and grid power. Fig. 2 shows the configuration of DG power system with control algorithm based proposed PM strategy. Proposed solutions (improved PNS extractor and existing PLLs, conventional control strategy, proposed RCG based control algorithm and various PM scenarios) are tested in grid connected DG based three phase inverter as shown in Fig. 2.

2.1. PV cell power generation

The measured power from single PV cell is relatively small. To generate more power, the various topologies of PV modules in series and parallel connection are required. The equivalent circuit of single PV cell is given in Fig. 1 (AbdelHady, 2017).

The PV has modeled and analyzed based on simple equivalent circuit. The characteristics of PV current and voltage are derived from Eq. (1) that depends on temperature and radiation. The PV power from boost converter output is calculated in (2) (AbdelHady, 2017; Bai, Abedi, & Lee, 2016).

$$I_{pv} = I_{ph}\left(1 + C_0\left(T - 273.15\right)\right) - I_o\left(e^{\frac{q(V_{pv}+I.R_s)}{nkT}} - 1\right) - \frac{(V_{pv}+I.R_s)}{R_{sh}} \tag{1}$$

$$P_{pv} = \eta_{boost\_conv} V_{pv} I_{pv} \tag{2}$$

where R_s is the series resistance, I_{ph} is the photon current, R_{sh} is shunt resistance, V_{pv} is open circuit voltage, T is temperature, k is Boltzmann's constant, I_o is reverse saturation current, q is the charge of an electron and η_{boost_conv} is efficiency of boost converter.

Table 1
List of nomenclatures.

Nomenclatures			
DG	Distributed Generation	MVF	Multivariable Filter
RES	Renewable Energy Sources	SRF	Synchronous Reference Frame
WT	Wind Turbines	MCCF	Multi Complex Coefficient Filter
PV	Photovoltaic Cell	TOSSI	Third Order Sinusoidal Integrator
FC	Fuel Cell	DAF	Dual Adaptive Filter
PM	Power Management	FOPI	Fractional Order Proportional Integral
PNS	Positive And Negative Sequence	FFT	Fast Fourier Transform
FCP	Flexible Control Parameter	DFT	Discrete Fourier Transform
DSC	Delay Signal Cancelation	STRF	Stationary Reference Frame
DSRF	Double Synchronous Reference	RCG	Reference Current Generator
DDSRF	Decoupled Double Synchronous Reference	DSOGI	Dual Second-Order Generalized Integrator
MAF	Moving Average Filter	THD	Total Harmonic Distortion
PR	Proportional Resonant	DB	Dead-beat
MW	Megawatt	ΔP	Remaining Power or Excess Power

2.2. Wind power generation

The wind kinetic energy is extracted by wind turbines with transferring the momentum of the air passing via the wind turbine rotor blades. The mechanical model of the permanent magnet synchronous generator (PMSG) is used in wind power system. The kinetic energy E is function of the flowing air mass m and velocity V_w can be expressed as follows Smaoui and Krichen (2016);

$$E = \frac{1}{2} m V_w^2 \tag{3}$$

The measured maximum power from wind turbine is limited by Betz law. With more high wind speed, it is obtained more energy. v_a and v_b, input and output speed from turbine blades, respectively. The wind power captured by a wind turbine is proportional to the rotor swept area A_s, the air mass density ρ_{air} and the wind speed V_w (Zaibia, Champenoisa, Roboamc, et al., 2018). Available input and **output turbine power** P_{wt_in} and P_{wt_out} are given with (4) and (5), respectively (Rashid, 2014).

$$P_{wt\_in} = \frac{1}{2} A_s \rho_{air} v_a^3 \tag{4}$$

$$P_{wt\_out} = \frac{dE}{dt} = \frac{1}{2} A_s \rho_{air} V_w^3 = \frac{1}{2} A_s \rho \left(\frac{v_a + v_b}{2} \right) \left(v_a^2 - v_b^2 \right) \tag{5}$$

To estimate the output power of wind turbine, the power is limited by a coefficient of power C_p. In order to simplify model, the optimal value is used for coefficient of power, such as $C_p = C_{p,op}$ (Zaibia et al., 2018). The maximum WT power based on power coefficient is also given as follows;

$$P_{wt\_out} = \frac{1}{2} C_{p,op}(\lambda, \beta) A_s \rho_{air} V_w^3 \tag{6}$$

Wind turbine rotor power coefficient C_p is generally a nonlinear function of tip speed ratio λ **and** blade pitch angle β;

$$C_p(\lambda, \beta) = 0.5176 \left(\frac{116}{\lambda_i} - 0.4\beta - 5 \right) e^{-\frac{21}{\lambda_i}} + 0.0068\lambda \tag{7}$$

$$\frac{1}{\lambda_i} = \frac{1}{\lambda + 0.08\beta} - \frac{0.035}{1 + \beta^3} \tag{8}$$

The maximum rotor power efficiency is not greater than Betz limit value (0.593).

2.3. Fuel cell power generation

Hydrogen based FC stacks generates electricity by way of the reaction between hydrogen and oxygen. The electrochemical model of the FC stack is presented based on mathematical calculation. Nernst equation is used to calculate FC output voltage V_{fc} with (9) (Chen, Yang, Deng, et al., 2017).

$$V_{fc} = N \left(E_0 + \frac{R.T}{2F} \left(In \frac{P_{H_2} P_{O_2}^{0.5}}{P_{H_2O}} \right) \right) - r_{ohmic} I_{fc} \tag{9}$$

where E_0 is standard reversible cell potential, r_{ohmic} is internal resistance, I_{fc} is FC stack current, N is number of cells, R is universal gas constant, T is temperature, F is Faraday's constant, P_{O_2} is pressure of oxygen, P_{H_2} is pressure of hydrogen and P_{H_2O} is pressure of water. The ohmic losses are neglected. The FC current and pressure of gases (hydrogen and oxygen) affect FC voltage. The reference current I_{ref} and fuel cell stack current I_{fc} is given as follows Chen et al. (2017). After reference current I_{ref} (10) is derived from FC stack voltage and reference power P_{ref}, FC stack current is obtained by (11).

$$I_{ref} = \frac{P_{ref}}{V_{fc}} \tag{10}$$

$$I_{fc} = \frac{I_{ref}}{1 + \tau_e . s} \tag{11}$$

The power supplied from FC stack is given as follows;

$$P_{fc} = N V_{fc} I_{fc} \tag{12}$$

3. Extraction of positive–negative sequences for reference current

3.1. FFT based PNS extractor

The fast Fourier transform (FFT) based harmonic detection technique is used to obtain the components of the grid voltage. The FFT consists of small discrete Fourier transform (DFT) pieces which has a rapid response due to less complex calculations and superior selectively filtering properties (Liu, Hu, Chen, et al., 2018; Saribulut, Teke, & Tümay, 2013). However, the DFT is influenced by frequency variations and induce one cycle delay compared with proposed DAF-PLL. The PNS voltage and harmonic components are separated in Fig. 3a and b, respectively. The mathematical calculation of the DFT is written in following.

$$V[k] = \sum_{n=0}^{N-1} v(n) w^{kn} \tag{13}$$

where harmonic frequency index $k = 1, 2, \ldots, N-1$ and N is number of sampling points. The voltage samples are categorized as even samples *(2n)* and odd samples $(2n+1)$. The magnitude of voltage for $k = 1$ is calculated as follows.

$$V[k] = \sum_{n=0}^{\frac{N}{2}-1} v(2n) w_{\frac{N}{2}}^{kn} + w^k \sum_{n=0}^{\frac{N}{2}-1} v(2n+1) w_{\frac{N}{2}}^{kn} \tag{14}$$

3.2. Proposed PNS extractor

Non-linear Adaptive Filters (AF) ensures fast tracking amplitude and phase angle of the input signal in grid connected systems. This filter provides many advantages, such as including generality, less complexity and computational burden and near optimum performance, even under non-stationary and asymmetry conditions (Meral, Cuma,

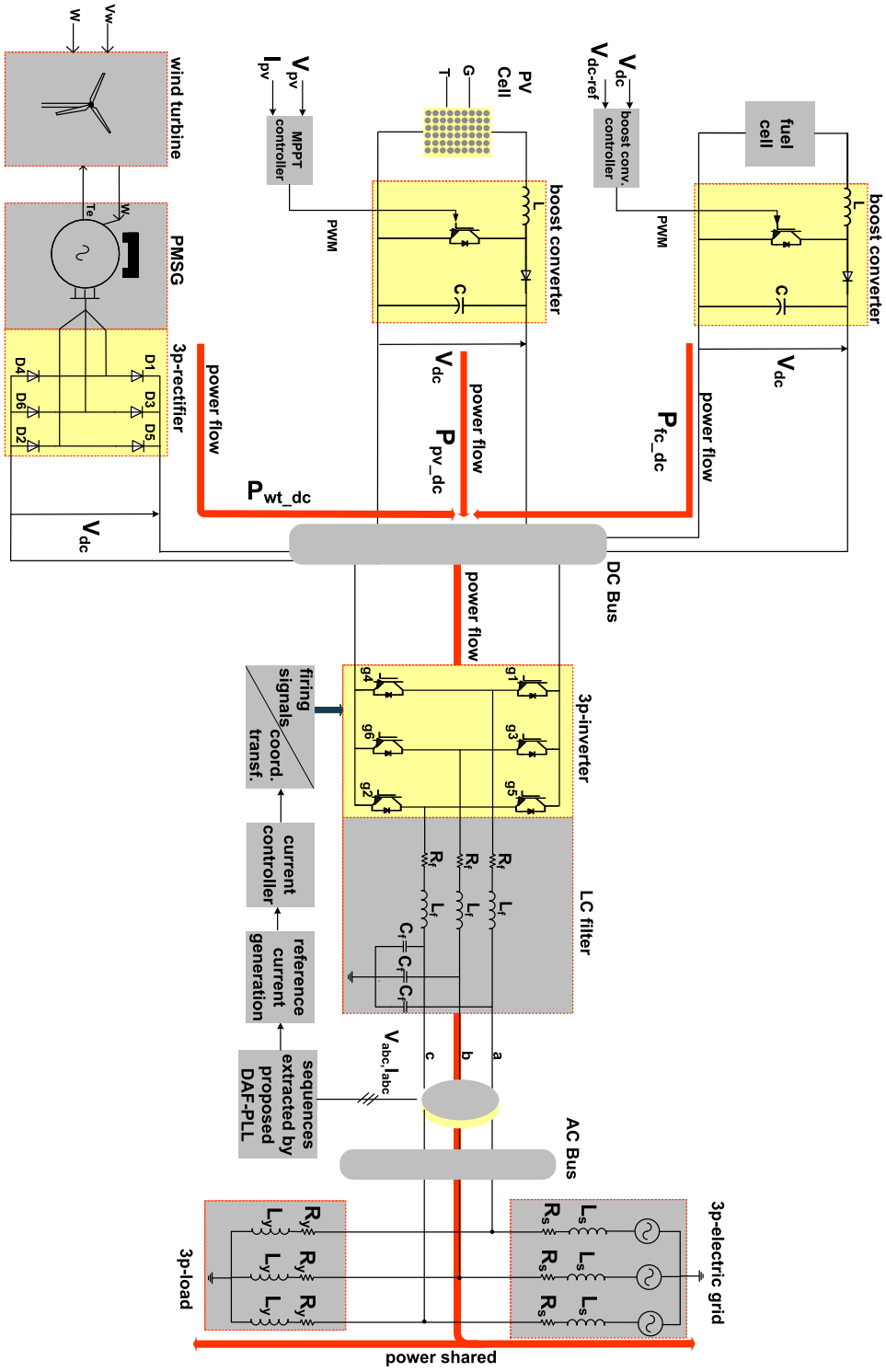

Fig. 2. The proposed configuration of DG power system.

Teke, et al., 2014). To overcome the drawbacks of the classical PLL and other advanced PLLs in literature, a new improved PLL method based on adaptive filter ensures fast dynamic response and removes ripple errors under adverse grid conditions in this paper. Non-linear Adaptive Filters based PLL is proposed in single phase system (Karimi-Ghartemani & Iravani, 2002). However, implementation of PLL in three phase system and obtaining orthogonal signals are not discussed. The advantage of proposed PLL over single phase adaptive filter based PLL is that it offers a separation for PNS components and an implementation in single and three phase system. The obtained PNS signals from improved dual adaptive filter based PLL (DAF-PLL) have been used to generate reference current signals. The improved single phase AF-PLL extracts component of the input signal V_p as the output signal V_α, its amplitude Apl and phase θ. The phase error is calculated deviation of the input signal from the output signal (Karimi-Ghartemani & Iravani, 2002). The proposed PLL can be applied to the single and three phase applications (see Fig. 4).

Where w and θ is estimated frequency and angle of proposed DAF-PLL. The output V_α is in phase with input signal V_p. The orthogonal $V_{q\alpha}$ voltage lags V_α by 90^0. The following Eqs. (15)–(17) in discrete time are

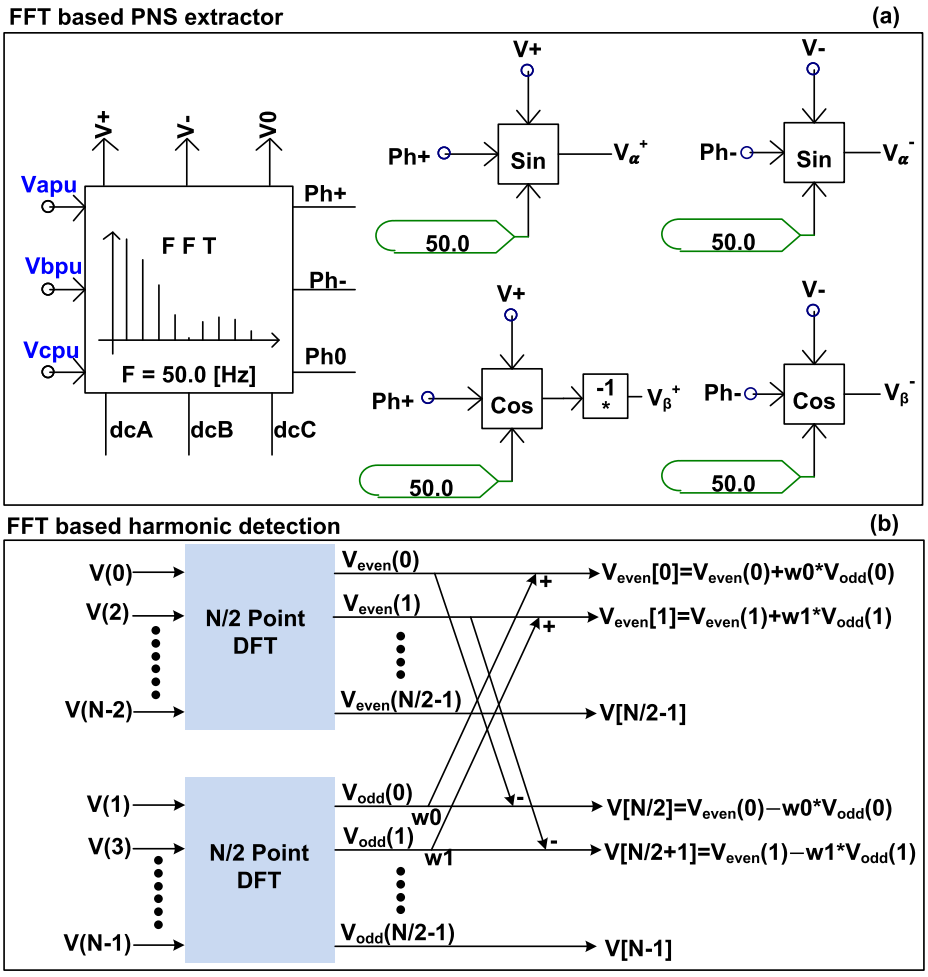

Fig. 3. The using FFT for, (a) separation of PNS components (b) harmonic detection.

used for the nonlinear AF based PLL.

$$Apl\,(t+1) = Apl\,(t) + k_1 e\,(t)\sin\left(\theta\,(t) - \frac{\pi}{2}\right) \tag{15}$$

$$\theta\,(t+1) = \theta\,(t) + k_p k_v e\,(t)\sin\left(\theta\,(t)\right) + w\,(t) \tag{16}$$

The output signals of proposed PLL are termed as V_α and $V_{q\alpha}$ which are given as follows,

$$\begin{aligned} V_\alpha\,(t) &= Apl\,(t)\sin\left(\theta\,(t) - \frac{\pi}{2}\right) \\ V_{q\alpha}\,(t) &= -Apl\,(t)\cos\left(\theta\,(t) - \frac{\pi}{2}\right) \end{aligned} \tag{17}$$

The obtained PNS voltage components in STRF are separated and also given based on SRF in following.

$$\begin{bmatrix} V_\alpha^+ = V_\alpha - qV_\beta \\ V_\beta^+ = qV_\alpha + V_\beta \\ V_\alpha^- = V_\alpha + qV_\beta \\ V_\beta^- = -qV_\alpha + V_\beta \end{bmatrix} = \begin{bmatrix} v^+\sin\left(wt + \theta_p\right) \\ -v^+\cos\left(wt + \theta_p\right) \\ v^-\sin\left(wt + \theta_n\right) \\ v^-\cos\left(wt + \theta_n\right) \end{bmatrix} \tag{18}$$

where positive phase angle θ_p represents as θ and negative phase angle θ_n represents as $-\theta$. The obtained PNS voltage components from proposed DAF-PLL in STRF are converted to SRF in following (19) and (20).

$$\begin{bmatrix} v_d^+ \\ v_q^+ \end{bmatrix} = \begin{bmatrix} \cos\left(\theta\,(t)\right) & \sin\left(\theta\,(t)\right) \\ -\sin\left(\theta\,(t)\right) & \cos\left(\theta\,(t)\right) \end{bmatrix} \begin{bmatrix} V_\alpha^+ \\ V_\beta^+ \end{bmatrix} \tag{19}$$

$$\begin{bmatrix} v_d^- \\ v_q^- \end{bmatrix} = \begin{bmatrix} \cos\left(\theta\,(t)\right) & -\sin\left(\theta\,(t)\right) \\ \sin\left(\theta\,(t)\right) & \cos\left(\theta\,(t)\right) \end{bmatrix} \begin{bmatrix} V_\alpha^- \\ V_\beta^- \end{bmatrix} \tag{20}$$

where V_{dq+} and V_{dq-} are the PNS voltage components. The relationship between PNS voltage (d-q) signals are written in following.

$$\begin{aligned} v_d &= v_d^+ + jv_d^- \\ v_q &= v_q^+ + jv_q^- \\ v^+ &= v_d^+ + jv_q^+ \\ v^- &= v_d^- + jv_q^- \end{aligned} \tag{21}$$

The orthogonal d-q signals derived from improved DAF-PLL can be significantly effective way to generate reference current for removing power oscillations (ripple errors) on control signals in STRF or SRF.

The gain parameters k_1, k_p and k_v are selected as optimal value for dynamic response of proposed PLL. The following items are indicated for tuning parameters.

- Increasing the value of k_1 increases dynamic response. However, it leads to oscillations on signals.
- With decreasing k_1, k_p and k_v, the magnitude of voltage/current peak is insensitive and highly robust to the undesirable variations and noise in the input signal (Karimi-Ghartemani & Iravani, 2002).

Performance comparisons of proposed PNS extractor are carried out under phase-to-phase fault and voltage swell as shown in Fig. 5. At 0.2 s and during eight cycles (80 ms), phase A has rated voltage and the voltages of phase B and phase C are decreased by 35% and at 0.34 s and during (50 ms), three phases are increased at 65% of their nominal values. The results verify that the proposed DAPLL exhibits superior performance to achieve fast tracking phase, shorter settling time of voltages tuning and reduce voltages ripple errors on PNS signals by means of comparisons of FFT.

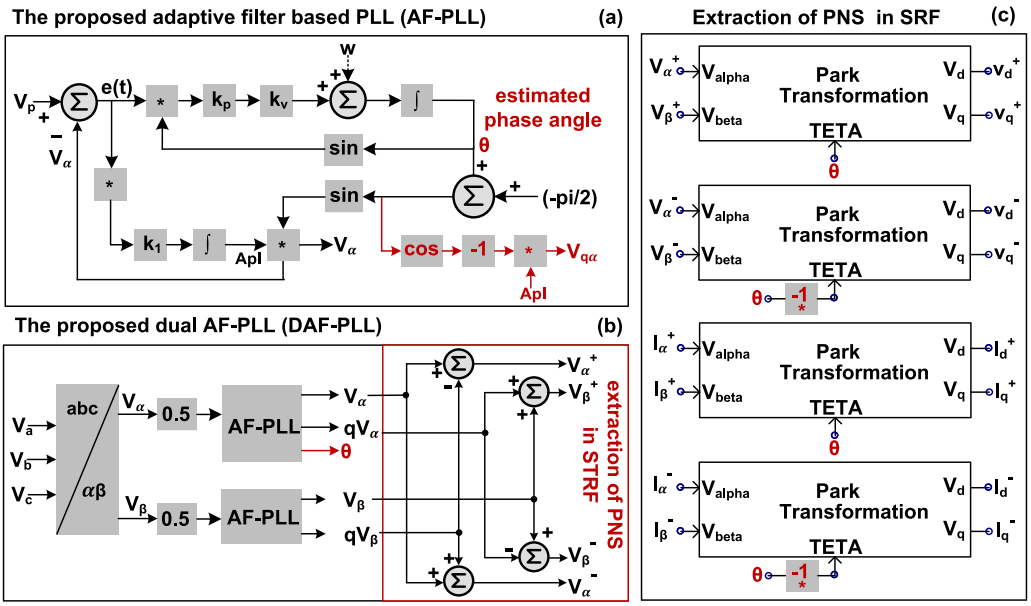

Fig. 4. The implementation of proposed PNS extractor; (a) in single-phase system, (b) in a three-phase system and (c) using for extraction of PNS signals.

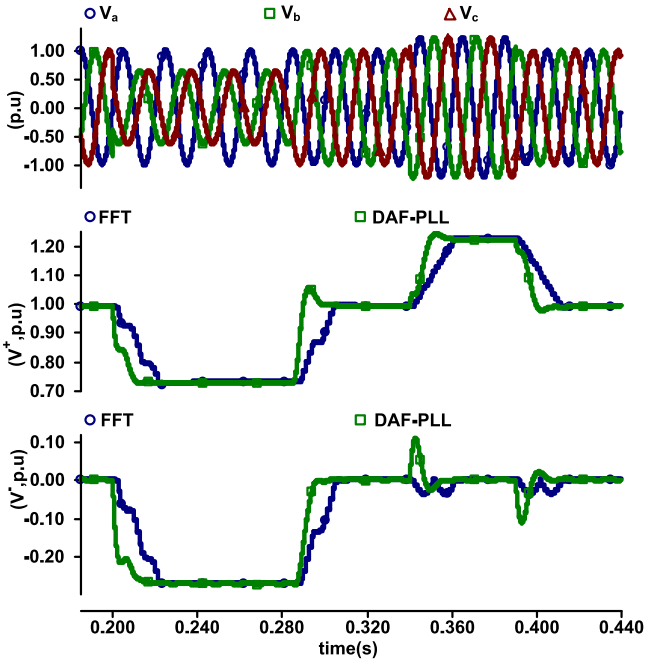

Fig. 5. The impact of phase to phase fault and voltage swell on PNS extractors.

3.3. Performance comparison of PNS extractors

To highlight the features of the proposed DAPLL, brief transient performance comparison with some PNS extractors are given in Table 2. As given in Table 2, among the mentioned methods, DSC-PLL and MVF-PLL has the lowest dynamic response. On the other hand, the DSOGI provides much simpler structure for PNS extractor but, relatively slower response than proposed DAF-PLL. The MCCF-PLL has the transient response comparable with the TOSSI-PLL and DDSRF. The results show that the proposed DAF-PLL exhibit the fastest transient response, lower settling time and better removing ripple errors on PNS components compared with existing PNS extractors.

4. Problem statement

This section presents the problem statement, which comprises of the RCG based conventional control strategy, problem formulation for active and reactive power oscillations and the proposed flexible RCG based controller for maximum power delivery and PM strategy. Firstly, conventional control strategy, are developed and analyzed and then, the active–reactive power and their oscillations are regulated and formulated and proposed solution is presented. To highlight performances of proposed solution, various control strategies are selected and compared.

4.1. Conventional RCG based controller

The negative sequences in conventional RCG are not taken into consideration. Hence, this lead to oscillations on control signals. Active and reactive power can be derived from principle of instantaneous power (Kabiri et al., 2016; Yang, Blaabjerg, Wang, et al., 2016).

$$\begin{aligned} P &= v_d i_d + v_q i_q \\ Q &= v_q i_d - v_d i_q \end{aligned} \tag{22}$$

As given in (23) and (24), both the active and reactive power oscillations are uncontrolled and the negative sequence current references cause the oscillations on control signals:

$$\begin{bmatrix} I^+_{dref} \\ I^+_{qref} \end{bmatrix} = \begin{bmatrix} +v^+_d & +v^+_q \\ +v^+_q & -v^+_d \end{bmatrix}^{-1} \begin{bmatrix} P_{ref} \\ Q_{ref} \end{bmatrix} \tag{23}$$

$$\begin{bmatrix} I^+_{dref} \\ I^+_{qref} \end{bmatrix} = \begin{bmatrix} \dfrac{+v^+_d}{\left(v^+_d\right)^2+\left(v^+_q\right)^2} & \dfrac{+v^+_q}{\left(v^+_d\right)^2+\left(v^+_q\right)^2} \\ \dfrac{+v^+_q}{\left(v^+_d\right)^2+\left(v^+_q\right)^2} & -\dfrac{+v^+_d}{\left(v^+_d\right)^2+\left(v^+_q\right)^2} \end{bmatrix} \begin{bmatrix} P_{ref} \\ Q_{ref} \end{bmatrix} \tag{24}$$

4.2. Problem formulation

The proposed PNS extractor based RCG provides constant power at rated inverter capacity. The injected active and reactive powers and their oscillations are regulated with some control objectives. The power oscillations are controlled by one FCP, which is employed for designation of active and reactive power oscillations. The formulation

Table 2
Performance comparison of transient response of PNS extractors.

PNS extractors	Response time	Sources
DSC-PLL	>60 ms	Meral (2012)
MVF-PLL	60 ms	Meral and Çelik (2018a)
DSOGI-PLL	>40 ms	Ali et al. (2017)
MCCF-PLL	40 ms	Guo et al. (2011)
TOSSI-PLL	40 ms	Chilipi et al. (2016)
DDSRF	40 ms	Rodriguez and Pou et al. (2007)
FFT	20 ms	
DAF-PLL	14 ms	

active–reactive power components and their oscillations can be written as follows (Kabiri et al., 2016; Zheng, Laijun, Yan, et al., 2018);

$$\begin{bmatrix} P \\ Q \\ P_s \\ P_c \\ Q_s \\ Q_c \end{bmatrix} = \begin{bmatrix} +v_d^+ & +v_q^+ & +v_d^- & +v_q^- \\ +v_q^+ & -v_d^+ & +v_q^- & -v_d^- \\ +v_d^- & +v_q^- & +v_d^+ & +v_q^+ \\ +v_q^- & -v_d^- & -v_q^+ & +v_d^+ \\ +v_q^- & -v_d^- & +v_q^+ & -v_d^+ \\ -v_d^- & -v_q^- & +v_d^+ & +v_q^+ \end{bmatrix} \begin{bmatrix} I_d^+ \\ I_q^+ \\ I_d^- \\ I_q^- \end{bmatrix} \tag{25}$$

P and Q are active and reactive powers that injected power to grid, respectively. P_s, P_c, Q_s and Q_c are amplitudes of active and reactive power oscillations caused by unbalance voltage and termed as double frequency oscillations. P_s and Q_s are related with $\sin(2wt)$ term and P_c and Q_c are related with $\cos(2wt)$ term. The proposed DAF-PLL based reference current signals can be derived as follows (Zheng et al., 2018);

$$\begin{bmatrix} I_{dref}^+ \\ I_{qref}^+ \\ I_{dref}^- \\ I_{qref}^- \end{bmatrix} = \begin{bmatrix} +v_d^+ & +v_q^+ & +v_d^- & +v_q^- \\ +v_q^+ & -v_d^+ & +v_q^- & -v_d^- \\ +v_d^- & +v_q^- & +v_d^+ & +v_q^+ \\ +v_q^- & -v_d^- & -v_q^+ & +v_d^+ \\ +v_q^- & -v_d^- & +v_q^+ & -v_d^+ \\ -v_d^- & -v_q^- & +v_d^+ & +v_q^+ \end{bmatrix}^{-1} \begin{bmatrix} P \\ Q \\ P_s \\ P_c \\ Q_s \\ Q_c \end{bmatrix} \tag{26}$$

The only active power oscillations can be controlled with deleting last two rows of (25).

$$\begin{bmatrix} I_{dref}^+ \\ I_{qref}^+ \\ I_{dref}^- \\ I_{qref}^- \end{bmatrix} = \begin{bmatrix} +v_d^+ & +v_q^+ & +v_d^- & +v_q^- \\ +v_q^+ & -v_d^+ & +v_q^- & -v_d^- \\ +v_d^- & +v_q^- & +v_d^+ & +v_q^+ \\ +v_q^- & -v_d^- & -v_q^+ & +v_d^+ \end{bmatrix}^{-1} \begin{bmatrix} P_{ref} \\ Q_{ref} \\ 0 \\ 0 \end{bmatrix} \tag{27}$$

Active and reactive power references P_{ref} and Q_{ref} are commanded to set constant power values for a desired level of inverter capacity. P_{ref} is selected as 1 per unit (p.u) and Q_{ref} is selected as 0, in order to inject maximum active power and minimum reactive power grid under grid faults.

$$\begin{bmatrix} I_{dref}^+ \\ I_{qref}^+ \\ I_{dref}^- \\ I_{qref}^- \end{bmatrix} = \begin{bmatrix} +v_d^+/A & +v_q^+/B \\ +v_q^+/A & -v_d^+/B \\ -v_d^-/A & +v_d^-/B \\ -v_q^-/A & -v_d^-/B \end{bmatrix} \begin{bmatrix} P_{ref} \\ Q_{ref} \end{bmatrix} \tag{28}$$

A and B are represented in following.

$$\begin{aligned} A &= \left(v_d^+\right)^2 + \left(v_q^+\right)^2 - \left(v_d^-\right)^2 - \left(v_q^-\right)^2 \\ B &= \left(v_d^+\right)^2 + \left(v_q^+\right)^2 + \left(v_d^-\right)^2 + \left(v_q^-\right)^2 \end{aligned} \tag{29}$$

For injected active power with zero oscillations, reactive power oscillations will be occurred. The amplitudes of reactive power oscillations are given as follows;

$$\begin{bmatrix} Q_s \\ Q_c \end{bmatrix} = 2 \begin{bmatrix} \frac{v_d^+ v_q^- - v_d^- v_q^+}{A} & \frac{v_d^- v_d^+ + v_q^- v_q^+}{B} \\ -\frac{v_d^- v_d^+ + v_q^- v_q^+}{A} & \frac{v_d^+ v_q^- - v_d^- v_q^+}{B} \end{bmatrix} \begin{bmatrix} P_{ref} \\ Q_{ref} \end{bmatrix} \tag{30}$$

Similarly, for only reactive power oscillations, the middle two rows of (25) are removed.

$$\begin{bmatrix} I_{dref}^+ \\ I_{qref}^+ \\ I_{dref}^- \\ I_{qref}^- \end{bmatrix} = \begin{bmatrix} +v_d^+ & +v_q^+ & +v_d^- & +v_q^- \\ +v_q^+ & -v_d^+ & +v_q^- & -v_d^- \\ +v_q^- & -v_d^- & +v_q^+ & -v_d^+ \\ -v_d^- & -v_q^- & +v_d^+ & +v_q^+ \end{bmatrix}^{-1} \begin{bmatrix} P_{ref} \\ Q_{ref} \\ 0 \\ 0 \end{bmatrix} \tag{31}$$

$$\begin{bmatrix} I_{dref}^+ \\ I_{qref}^+ \\ I_{dref}^- \\ I_{qref}^- \end{bmatrix} = \begin{bmatrix} +v_d^+/A & +v_q^+/B \\ +v_q^+/A & -v_d^+/B \\ +v_d^-/A & -v_q^-/B \\ +v_q^-/A & +v_d^-/B \end{bmatrix} \begin{bmatrix} P_{ref} \\ Q_{ref} \end{bmatrix} \tag{32}$$

Amplitudes of active power oscillations are obtained with (25) and (32) as follows;

$$\begin{bmatrix} P_s \\ P_c \end{bmatrix} = 2 \begin{bmatrix} \frac{v_d^- v_d^+ + v_q^- v_q^+}{B} & \frac{v_d^- v_q^+ - v_d^+ v_q^-}{A} \\ \frac{v_d^+ v_q^- - v_d^- v_q^+}{B} & \frac{v_d^- v_d^+ + v_q^- v_q^+}{A} \end{bmatrix} \begin{bmatrix} P_{ref} \\ Q_{ref} \end{bmatrix} \tag{33}$$

The power oscillations are shared between active and reactive powers. The combined with amplitudes of active and reactive power oscillations can be written in following (Kabiri et al., 2016);

$$\begin{bmatrix} P_s \\ P_c \\ Q_s \\ Q_c \end{bmatrix} = \begin{bmatrix} \frac{v_d^- v_d^+ + v_q^- v_q^+}{\left(v_d^+\right)^2 + \left(v_q^+\right)^2} & \frac{v_d^- v_q^+ - v_d^+ v_q^-}{\left(v_d^+\right)^2 + \left(v_q^+\right)^2} \\ \frac{v_d^+ v_q^- - v_d^- v_q^+}{\left(v_d^+\right)^2 + \left(v_q^+\right)^2} & \frac{v_d^- v_d^+ + v_q^- v_q^+}{\left(v_d^+\right)^2 + \left(v_q^+\right)^2} \\ \frac{v_d^+ v_q^- - v_d^- v_q^+}{\left(v_d^+\right)^2 + \left(v_q^+\right)^2} & \frac{v_d^- v_d^+ + v_q^- v_q^+}{\left(v_d^+\right)^2 + \left(v_q^+\right)^2} \\ -\frac{v_d^- v_d^+ + v_q^- v_q^+}{\left(v_d^+\right)^2 + \left(v_q^+\right)^2} & \frac{v_d^+ v_q^- - v_d^- v_q^+}{\left(v_d^+\right)^2 + \left(v_q^+\right)^2} \end{bmatrix} \begin{bmatrix} P_{ref} \\ Q_{ref} \end{bmatrix} \tag{34}$$

The combined with active and reactive power oscillations are controlled by one FCP k. when k is close to 1, active power oscillations increase. Similarly, when k is close to −1, reactive power oscillations increase.

$$\begin{bmatrix} I_{dref}^+ \\ I_{qref}^+ \\ I_{dref}^- \\ I_{qref}^- \end{bmatrix} = \begin{bmatrix} +v_d^+/A' & +v_q^+/B' \\ +v_q^+/A' & -v_d^+/B' \\ -kv_d^-/A' & +kv_q^-/B' \\ -kv_q^-/A' & -kv_d^-/B' \end{bmatrix} \begin{bmatrix} P_{ref} \\ Q_{ref} \end{bmatrix} \tag{35}$$

where A' and B' are represented in following.

$$\begin{aligned} A' &= \left(v_d^+\right)^2 + \left(v_q^+\right)^2 - k\left[\left(v_d^-\right)^2 + \left(v_q^-\right)^2\right] \\ B' &= \left(v_d^+\right)^2 + \left(v_q^+\right)^2 + k\left[\left(v_d^-\right)^2 + \left(v_q^-\right)^2\right] \end{aligned} \tag{36}$$

where $I_{dref} = I_{dref}^+ + I_{dref}^-$ and $I_{qref} = I_{qref}^+ + I_{qref}^-$. The interval control parameter k is $[-1, 1]$.

5. The proposed flexible RCG based controller for maximum power delivery and PM strategy

The RCG is considerably crucial that determine the performances of the grid connected three phase inverter during grid faults. The

maximum active and minimum reactive powers are achieved by the RCG. However, to keep maximum power at level of inverter capacity, the inverter current requires increasing. The current references for active and reactive powers are calculated by PNS voltage components in STRF and given in (37) and (38).

$$\begin{aligned} I_{\alpha(p)} &= \frac{2}{3}\frac{P_{ref}}{\left[(v_\alpha^+)^2+\left(v_\beta^+\right)^2+k(v_\alpha^-)^2+\left(v_\beta^-\right)^2\right]}\left[v_\alpha^+ + kv_\alpha^-\right] \\ I_{\beta(p)} &= \frac{2}{3}\frac{P_{ref}}{\left[(v_\alpha^+)^2+\left(v_\beta^+\right)^2+k(v_\alpha^-)^2+\left(v_\beta^-\right)^2\right]}\left[v_\beta^+ + kv_\beta^-\right] \end{aligned} \tag{37}$$

$$\begin{aligned} I_{\alpha(q)} &= \frac{2}{3}\frac{Q_{ref}}{\left[(v_\alpha^+)^2+\left(v_\beta^+\right)^2+k(v_\alpha^-)^2+\left(v_\beta^-\right)^2\right]}\left[v_\beta^+ + kv_\beta^-\right] \\ I_{\beta(q)} &= \frac{2}{3}\frac{Q_{ref}}{\left[(v_\alpha^+)^2+\left(v_\beta^+\right)^2+k(v_\alpha^-)^2+\left(v_\beta^-\right)^2\right]}\left[-v_\alpha^+ - kv_\alpha^-\right] \end{aligned} \tag{38}$$

P_{ref} and Q_{ref} are active and reactive power references and can be adjustable with inverter capacity. The active and reactive power current references based on PNS voltage components can be reformulated with only one FCP as given in (39) and (40) (Guo, Liu, & Lu, 2017).

$$\begin{aligned} I_{\alpha(p)} &= \frac{2}{3}\frac{P_{ref}}{\left[\|v^+\|^2+k\|v^-\|^2\right]}\left[v^+\sin\left(\theta_p\right)+kv^-\sin\left(\theta_n\right)\right] \\ I_{\beta(p)} &= \frac{2}{3}\frac{P_{ref}}{\left[\|v^+\|^2+k\|v^-\|^2\right]}\left[-v^+\cos\left(\theta_p\right)+kv^-\cos\left(\theta_n\right)\right] \end{aligned} \tag{39}$$

$$\begin{aligned} I_{\alpha(q)} &= \frac{2}{3}\frac{Q_{ref}}{\left[\|v^+\|^2+k\|v^-\|^2\right]}\left[-v^+\cos\left(\theta_p\right)+kv^-\cos\left(\theta_n\right)\right] \\ I_{\beta(q)} &= \frac{2}{3}\frac{Q_{ref}}{\left[\|v^+\|^2+k\|v^-\|^2\right]}\left[-v^+\sin\left(\theta_p\right)-kv^-\sin\left(\theta_n\right)\right] \end{aligned} \tag{40}$$

where $\|.\|$ is magnitude of vector. The total references current can be given as follows;

$$\begin{bmatrix} I_{\alpha ref} \\ I_{\beta ref} \end{bmatrix} = \begin{bmatrix} I_{\alpha(p)} + I_{\alpha(q)} \\ I_{\beta(p)} + I_{\beta(q)} \end{bmatrix} = \begin{bmatrix} M_1\sin\left(\theta_p-\delta_1\right)+M_2\sin\left(\theta_n-\delta_2\right) \\ -M_1\cos\left(\theta_p-\delta_1\right)+M_2\cos\left(\theta_n-\delta_2\right) \end{bmatrix} \tag{41}$$

where the PNS active–reactive power current components is detailed in (42).

$$\begin{aligned} I_{\alpha(p)} &= I_{\alpha(p^+)} + I_{\alpha(p^-)} \\ I_{\alpha(q)} &= I_{\alpha(q^+)} + I_{\alpha(q^-)} \\ I_{\beta(p)} &= I_{\beta(p^+)} + I_{\beta(p^-)} \\ I_{\beta(q)} &= I_{\beta(q^+)} + I_{\beta(q^-)} \end{aligned} \tag{42}$$

where M_1, M_2, δ_1 and δ_2 is given in (43) as follows;

$$\begin{aligned} M_1 &= \sqrt{\left[\frac{v^+P_{ref}}{\|v^+\|^2+k\|v^-\|^2}\right]^2+\left[\frac{v^+Q_{ref}}{\|v^+\|^2+k\|v^-\|^2}\right]^2} \\ \delta_1 &= \tan^{-1}\frac{Q_{ref}\left[\|v^+\|^2+k\|v^-\|^2\right]}{P_{ref}\left[\|v^+\|^2+k\|v^-\|^2\right]} \\ M_2 &= \sqrt{\left[\frac{kv^-P_{ref}}{\|v^+\|^2+k\|v^-\|^2}\right]^2+\left[\frac{kv^-Q_{ref}}{\|v^+\|^2+k\|v^-\|^2}\right]^2} \\ \delta_2 &= \tan^{-1}\frac{kQ_{ref}\left[\|v^+\|^2+k\|v^-\|^2\right]}{kP_{ref}\left[\|v^+\|^2+k\|v^-\|^2\right]} \end{aligned} \tag{43}$$

After processed reference current signals and injected current signals by fractional order proportional integral (FOPI) current regulation controller, the reference voltage signals $V_{\alpha ref}$ and $V_{\beta ref}$ are obtained. The FOPI controller is applied to (44). Compared with conventional PI and proportional resonant (PR) (Meral & Çelik, 2018b) controllers, the FOPI controller is preferred that can achieve zero steady-state error in STRF under unbalanced conditions. The current tracking errors are minimized and exhibit fast dynamic response. In particular, the PR current regulation is sensitive to frequency variation. The obtained reference voltages based on STRF for firing signals of three phase inverter are given as follows with (44). The proposed solution is illustrated in Fig. 6.

Table 3
Parameters for proposed test system.

Parameters		Values
DC bus voltage		800 V
Grid line-line voltage (rms)		380 V
Grid frequency		50 Hz
LC filter	L	0.5 mH
	C	50 μF
Load power		0.2–0.7 MW
$k_p = k_v$		30
k_1		0.31
λ		0.5
Switching frequency		2500 Hz

$$\begin{aligned} V_{\alpha ref} &= \left[I_{\alpha ref}-I_\alpha\right].[FOPI] = \left[I_{\alpha ref}-I_\alpha\right].\left[k_p+\frac{k_i}{s^\lambda}\right] \\ V_{\beta ref} &= \left[I_{\beta ref}-I_\beta\right].[FOPI] = \left[I_{\beta ref}-I_\beta\right].\left[k_p+\frac{k_i}{s^\lambda}\right] \end{aligned} \tag{44}$$

where k_p and k_i are gain of FOPI parameters and λ is fractional order of integrator.

6. Implementation of current controller based proposed PM strategy

The performance of current controller based proposed PM strategy are tested, analyzed and compared with conventional controller under balanced and unbalanced conditions in this section. The schematic diagram of proposed test system is given in Fig. 7. The proposed solution is developed and simulated by PSCAD/EMTDC software. The parameters for operation of proposed test system are summarized in Table 3.

The remaining power (ΔP) from DG the system is calculated by the difference among the DG units $P_{DG(P_{pv}+P_{wt}+P_{fc})}$, electric grid P_g and the load power demand P_L. The excess power ΔP is transmitted to the electric grid. The flowchart of the proposed PM strategy is shown in Fig. 7b.

To confirm availability and effectiveness of current controller based proposed PM strategy, they are tested under various cases such as starts up DG energy sources, variation of reference power, variation of load power, grid faults conditions and harmonic distortions in the DG system. The rated inverter capacity based the PM strategy depend on the magnitude of load power P_L and DG power production. The several PM strategies based (45) are written in following:

$$\Delta P = P_{[P_{pv}+P_{fc}+P_{wt}]} - P_L \tag{45}$$

- If $\Delta P < 0$ then the DG power production is not sufficient and grid power P_g should be operated.
- If $\Delta P = 0$ then the DG power production is sufficient and grid power P_g is not required to start-up.
- If $\Delta P > 0$ then the DG power production is sufficient and excess power P_{excess} is transmitted to grid. The excess power is calculated with $P_{excess} = \Delta P$.

The power balance between DG units at the DC bus (inverter input) and inverter output power P can be written as follows;

$$\eta_{\text{inv}}\left[\eta_{pv_{boost_{conv}}}P_{pv_{dc}}+\eta_{fc_{boost_{conv}}}P_{fc_{dc}}+\eta_{rec}P_{wt_{dc}}\right]-P-P_{losses}=0 \tag{46}$$

where P_{pv_dc}, P_{fc_dc} and P_{wt_dc} energy source powers are supplied by the PV, the FC and WT, respectively and power loses P_{losses} is consumed by three phase inverter. The $\eta_{inv} = 0.93$ is efficiencies of three phase inverter, $\eta_{pv\_boost\_conv} = 0.96$ is efficiencies of boost power in PV cell, $\eta_{fc\_boost\_conv} = 0.93$ is efficiencies of boost power in FC cell and $\eta_{rec} = 90$ is efficiencies of uncontrolled rectifier.

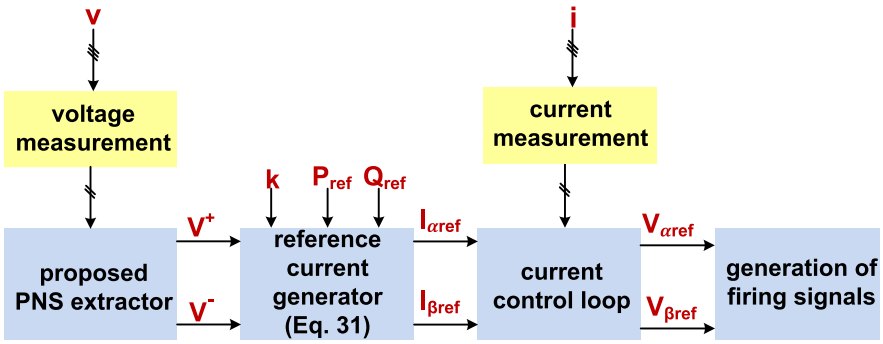

Fig. 6. Proposed reference current based controller.

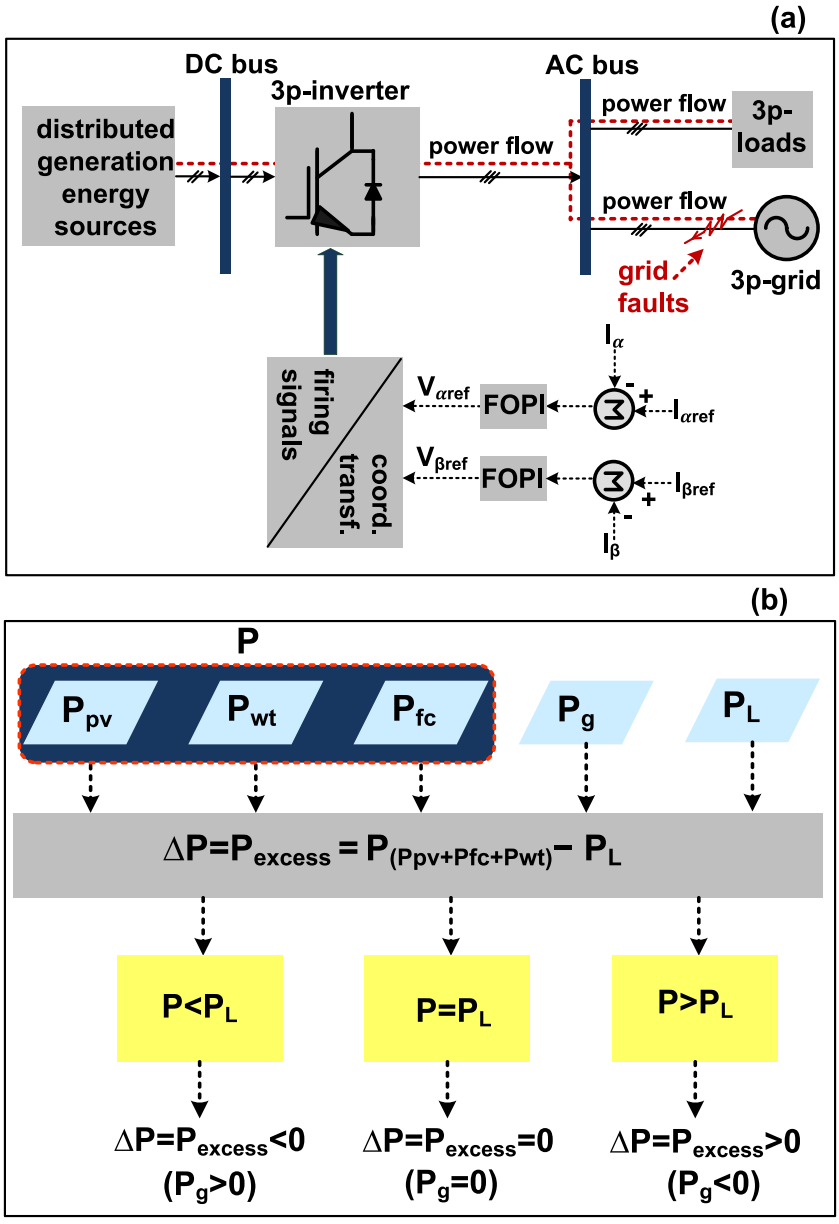

Fig. 7. The proposed entire test system consists of; (a) control of grid connected DG based 3p-inverter and (b) flowchart of the PM strategy.

6.1. Case 1: injection of low and high active power scenarios under balanced grid conditions

The DG energy sources start up at DC bus under different times. The PV cell, WT and FC energy sources have 0.117 MW, 0.11 MW and 0.29 MW power at DC bus, respectively as shown in Fig. 8a. PV cell, WT and FC energy sources have 0.108 MW, 0.1 MW and 0.27 MW power at inverter output, respectively. Fig. 8a depicts the power balanced between inverter total output power, electric grid and load power under start-up energy sources. When inverter output power is

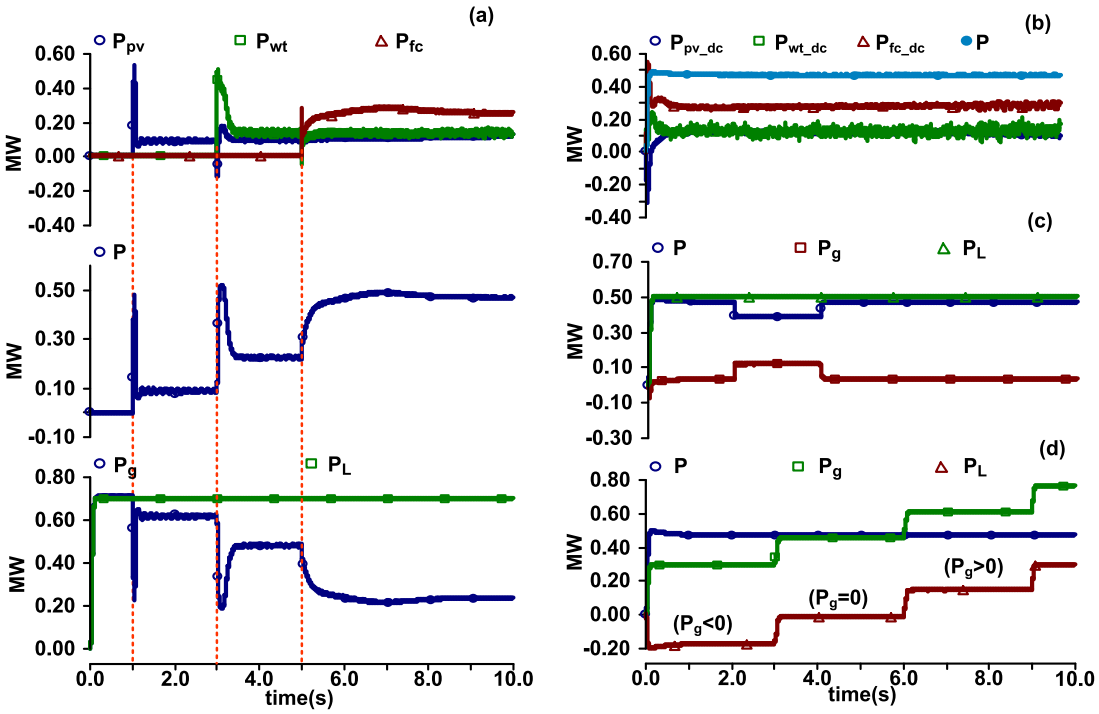

Fig. 8. The result for; (a) start–up energy sources, grid and load power at different times, (b) DG sources power and inverter total output power at DC bus, (c) variation of active power reference and (d) variation of load power demand.

increased, electric grid power is decreased, proportionally and vice versa. Injected total active power P from inverter output reaches total power of P_{pv}, P_{fc} and P_{wt} energy sources (0.47 MW) (see Fig. 8b).

The active power reference (inverter rated power) is reduced from 0.47 MW to 0.37 MW at 2 s. If DG sources supply less power such as; PV cell and WT depending on weather conditions or request reduction of power demand (in the even that energy sources are unable), this scenario can be occurred, as shown in Fig. 8c. The proposed control strategy applies active power curtailment to deal with surpass the maximum rated current and disconnection.

The variation of load demand between 0.3 MW and 0.75 MW is given in Fig. 8d as graphically. If load power demand P_L exceeds the available power generation from DG power system $P_{(P_{pv}+P_{fc}+P_{wt})}$, the grid will start up under variation loads. When DG power production exceeds load demand, excess active power is transmitted to the electric grid.

6.2. Case 2: the impact of phase to phase fault on controllers

The phase to phase grid fault is occurred at 0.3 s in Fig. 9. When the phase B and C voltage values are decreased at 65% of their nominal, electric grid and load powers are decreased, proportionally. In this case, it is possible observed that conventional control strategy supplies lower power than rated inverter capacity. As depicted in Fig. 9a, the inverter maximum rated power cannot be reached under grid faults. Therefore, the electric grid supplies more active power to load demand. The injected current has remarkably high total harmonic distortion (THD) values under when grid faults are occurred. Moreover, conventional control strategy is not deal with power oscillations. The results in Fig. 9b are reported that proposed controller delivers maximum active power without any oscillations under grid faults. The injected current has lower THD value about 1% by means of comparison of conventional control strategy. In proposed control strategy, the electric grid supplies less power to load demand by means of comparison of conventional control strategy

6.3. Case 3: the impact of phase to phase fault and harmonic distortions on controllers

As shown Fig. 10, the impact of both the phase to phase grid fault and 5th and 7th voltage harmonics are applied to three phase signals at 0.3 s. When phase B and C voltage values are decreased at 65% of their nominal, electric grid and load powers are decreased, proportionally. It is possible observed that injected active power by conventional control strategy is lower than desired maximum power delivery. Therefore, the electric grid supplies more power to load demand. The injected current has remarkably high total harmonic distortion (THD) values and double frequency oscillations of active–reactive power are occurred during grid faults in conventional control strategy. The results in Fig. 10b are reported that injected active power is maintained at constant power without any oscillations when utilizing proposed RCG based control algorithm. The less excess active power is transmitted to electric grid since the conventional control strategy cannot provide power generation at inverter rated power. The rated current injection becomes more balanced and amplitudes of power oscillations are considerably reduced by means of comparison of conventional control strategy.

6.4. Case 4: the impact of flexible control parameter (FCP) on proposed controller

The results are obtained in Fig. 11a by sweeping the flexible control parameter (FCP) k. It is clearly seen that active and reactive powers are controlled with only one FCP, k. When control parameter k is close to 1, the amplitudes of active power oscillations increase and reactive power oscillations decrease. However, active power oscillations cause the second order voltage ripple in DC link voltage. This DC link voltage ripple results in undesired third-order harmonic in the grid side, at same time. With control parameter is equal to -1, there is no oscillation on active power. It is expected that oscillations seem on reactive power. The injected current is unbalanced with $k = 1$ and -1 and injected current is balanced with $k = 0$. When The proposed RCG based controller achieves constant active power with controllable oscillations at rated inverter capacity under grid faults. One of the important features of proposed

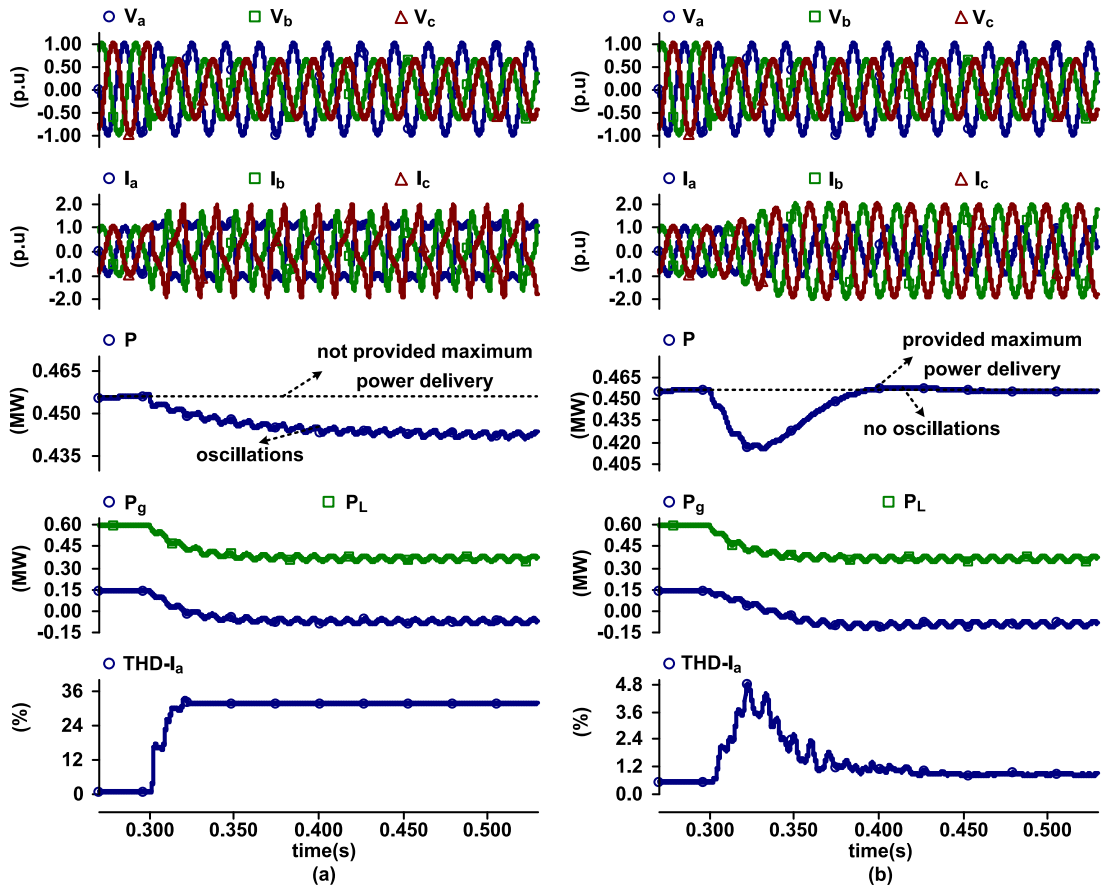

Fig. 9. The results for; (a) conventional and (b) proposed controllers under phase to phase grid faults.

flexible control strategy is that active and reactive power oscillations are regulated and controlled by only one FCP, k by means of comparison of previous studies such as Guo et al. (2017) and Sosa et al. (2016).

As shown in Fig. 11b, another approach has been carried out that maximum active power and minimum reactive power delivery capabilities are injected into grid. Phase to phase grid fault occurs from 0.3 s to 0.4 s (five cycles) with phase B and phase C are decreased by %35. It can be seen that positive sequence active current, I_p^+ is maximum and positive sequence reactive current, I_q^+ is minimum. The negative-sequence c of active and reactive currents, I_p^- and I_q^- are used to eliminate active and reactive power oscillations.

6.5. Performance comparison of proposed solution

Several control strategies have been reported in the literature. Performance comparisons in terms of the regulation of active and reactive power, controllability of active and reactive power oscillations, current regulation control, number of control parameters and PNS extractors of control strategies are exhibited in Table 4. Some studies on regulation of active power P or reactive power Q, or both of P and Q, by generating the PNS current references have been reported by Guo et al. (2017), Kabiri et al. (2016), Lopez et al. (2018), Reyes et al. (2012), Rodriguez, Timbus, Teodorescu and et al. (2007), Sosa et al. (2016) and Wang et al. (2010). Active and reactive power are regulated, but control of active and reactive oscillations are not discussed by Jin et al. (2017) and Rodriguez and Timbus et al. (2007). Another approach is mitigation of active–reactive power oscillations. Some previous studies (Jin et al., 2017; Reyes et al., 2012; Rodriguez and Timbus et al., 2007) have not dealt with both P and Q oscillations. However, only active power oscillations are eliminated by Lopez et al. (2018) and Sosa et al. (2016). Another problem is the design of current regulators for power quality improvement under unbalanced grid conditions. Various current regulators are presented to improve the transient and steady-state performance and reduce complexity control structures such as DSRF-PI (Jin et al., 2017; Kabiri et al., 2016) and DDSRF-PI (Reyes et al., 2012) current regulators in synchronous are complex, consist of four PI controllers and need multiple reference frame transformations. To regulate PNS quantities, only two STRF based PR controllers are used by Guo et al. (2017) and Wang et al. (2010). However, it is influenced by frequency variations. Dead-beat (DB) controller exhibits fast transient response, but it is sensitive to model parameters. Other approach is number of FCP. Decreasing number of control parameters provide better controllability of oscillations.

As shown in Table 4, the main contributions of proposed solution consist of: (1) active and reactive power regulation and minimizing both active and reactive power oscillation with only one FCP, (2) comparing with PI, PR, DB, DSRF-PI and DDSRF-PI current regulation, an advanced controller, FOPI is presented to regulate PNS components, (3) power flow among DG units is also discussed and (4) fast and robust improved DAF-PLL is proposed to separate PNS components and performance comparison of proposed DAF-PLL is also given in Table 2.

6.6. Numerical results for PM strategy

The proposed control strategy based various PM strategy is applied to the grid connected DG based three phase inverter. The proposed system is tested under start-up of DG sources, variation of active power reference, load and phase to phase fault conditions. The proposed controller provides constant power delivery at rated inverter capacity under grid faults. The proposed control algorithm based various PM scenarios in terms of injection low and high active power and suitability of energy sources are tested under balanced and unbalanced conditions.

Table 4
Performance comparison of proposed control strategy.

Control strategy	Regulation of P, Q	Control of P, Q oscillations	Current regulation	Number of FCP	PM strategy	PNS extractor
Rodriguez and Timbus et al. (2007)	P	No	DB	No	No	DSOGI-PLL
Wang et al. (2010)	P, Q	Yes	PR	1	No	MVF-PLL
Guo et al. (2017)	P, Q	Yes	PR	2	No	MCCF-PLL
Reyes et al. (2012)	No	No	DDSRF-PI	No	No	DSRF-PLL
Kabiri et al. (2016)	P, Q	Yes	DSRF-PI	1	No	DSOGI-PLL
Jin et al. (2017)	P, Q	No	DSRF-PI	No	No	DSC-PLL
Sosa et al. (2016)	P, Q	Only P	PR	2	No	DSOGI-PLL
Lopez et al. (2018)	P, Q	Only P	PR	2	No	DSOGI-PLL
Proposed control strategy	P, Q	Yes	FOPI	1	Yes	DAF-PLL

According to various cases, injected active power to grid, electric grid, load demand power and excess active power from power generation are given as numerical results in Table 5.

7. Conclusion and future work

This paper proposes a current controller based PM strategy for three phase inverter interfaced DG system to provide power balance among DG units, electric grid and load demand under balanced and unbalanced conditions. The PNS voltage and current components are extracted with proposed DAF-PLL, which ensures remarkably fast dynamic response to generate RCG. The proposed controller provides constant power at rated inverter capacity and enhances transfer capability of active and reactive power to electric grid with zero oscillations by means of comparison of conventional control strategy. The injected current has THD value about 1% compared with conventional control strategy. As shown in Table 2, proposed DAF-PLL exhibit the fastest transient response (less one cycle-14 ms) and better minimizing ripple errors on PNS components compared with existing PNS extractors (greater than one cycle-20 ms) in literature. Theoretical analyses of active and reactive power oscillations are comprehensive discussed with FCP.

All local current/power controllers for PV cell, FC and WT are designed to control the power flow among the DG components, separately. The proposed controller based various PM scenarios are developed to manage and distribute the power among the DG system units after taking into account the three energy source (PV, FC and WT) powers. Little attention has been paid to manage power flow and supply maximum power with injecting the maximum-rated current under grid faults in previous studies. The main contribution of this paper may be outlined in following:

- The proposed PM strategy fulfills active and reactive power regulation and maximize power deliver at rated inverter capacity.
- Compared with previous similar studies, maximum active power and minimum reactive power are injected into grid under grid faults.
- Both active and reactive power oscillations are minimized by only one FCP compared with previous similar studies.
- Fast and robust improved DAF-PLL is proposed to separate PNS components and to obtain the RCG.
- The FOPI current regulator is preferred to achieve zero steady state error and fast transient response instead of conventional controllers.
- Performance comparison of proposed control strategy and proposed PNS extractor are comprehensively tested and overviewed with previous studies.

The results of cases show that proposed control strategy exhibits superior performances for maximum power delivery capability and transmit excess active power to electric grid and load. Theoretical and simulation results have been verified the effectiveness, availability and robustness of the proposed solution. In continuation of this study, a proper experimental validation is challenging. However, real time hardware in loop can be performed. The following subjects can be suggested for future studies:

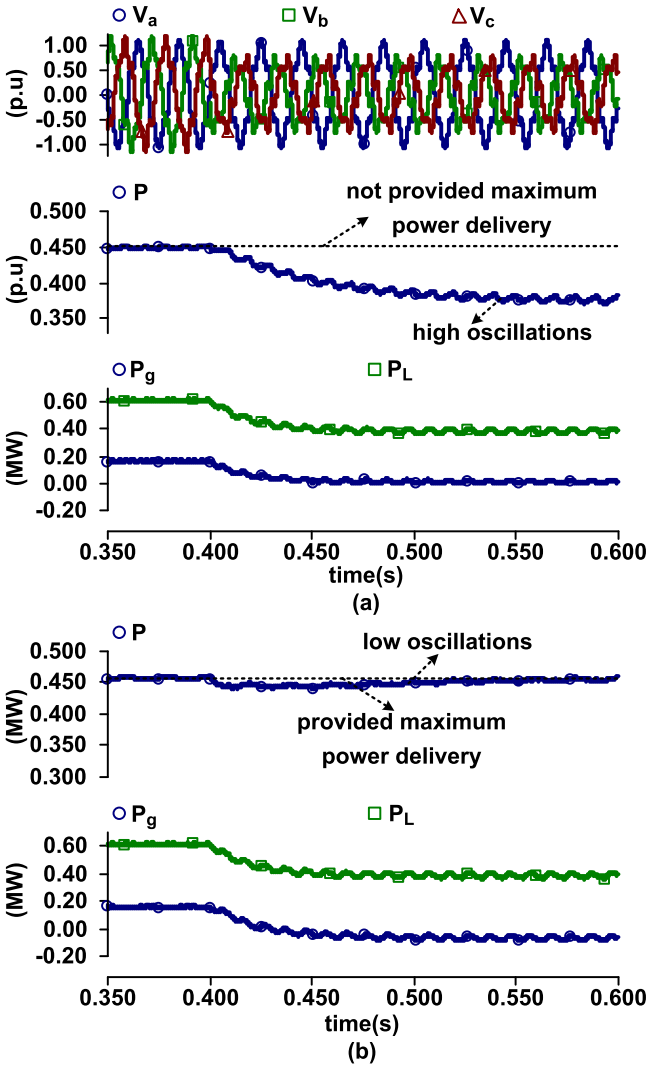

Fig. 10. The results for; (a) conventional control strategy and (b) proposed control strategy under phase to phase grid faults and harmonic distortions.

- More robust and less affected by harmonics, PNS extractor can be improved according to the proposed sequences extractors.
- Proposed PM strategy will be integrated into droop controller in parallel inverter.
- The selection of FCP is an open research topic for flexible control strategy and voltage support control.
- Stability, robustness and eigenvalues of proposed control strategy will be analyzed.
- Overcurrent phenomenon can be discussed for grid connected inverter systems under grid faults.

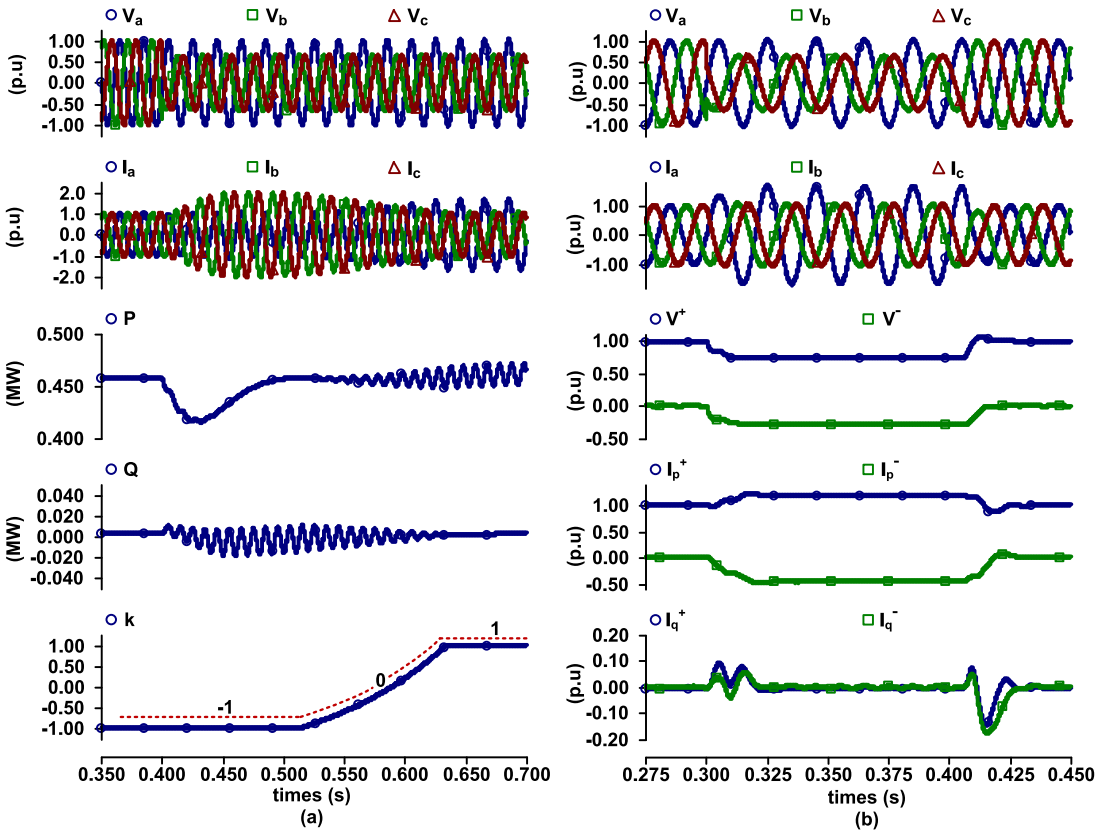

Fig. 11. The results for; (a) impact of FCP on active and reactive power oscillations and (b) maximum active current and minimum reactive current.

Table 5
Various PM scenarios for power flow balance.

Cases	Power flow balance			
Start-up DG sources	P_{DG}	P_g	P_L	P_{excess}
t = 1 s	P_{pv}	0.592 MW	0.7 MW	−0.592 MW
t = 3 s	$P_{pv} + P_{wt}$	0.492 MW	0.7 MW	−0.492 MW
t = 5 s	$P_{pv} + P_{wt} + P_{fc}$	0.222 MW	0.7 MW	−0.222 MW
Variation of active power reference	P_{DG}	P_g	P_L	P_{excess}
t = 1 s	0.47 MW	0.07 MW	0.4 MW	−0.07 MW
t = 2 s	0.37 MW	0.1 MW	0.4 MW	−0.1 MW
t = 4 s	0.47 MW	0.07 MW	0.4 MW	−0.07 MW
Variation of load power	P_L	P_g	P_{DG}	P_{excess}
t = 2 s	0.3 MW	−0.17 MW	0.47 MW	0.17 MW
t = 3 s	0.45 MW	0.0 MW	0.47 MW	0.02 MW
t = 6 s	0.6 MW	0.17 MW	0.47 MW	−0.17 MW
t = 9 s	0.75 MW	0.28 MW	0.47 MW	−0.28 MW
Phase to phase fault	P_L	P_g	P_{DG}	P_{excess}
Conventional controller	0.377 MW	−0.065 MW	0.442 MW	0. 065 MW
Proposed controller	0.377 MW	−0.078 MW	0.455 MW	0.078 MW
Phase to phase fault-harmonic distortions	P_L	P_g	P_{DG}	P_{excess}
Conventional controller	0.377 MW	0.005 MW	0.372 MW	−0.005 MW
Proposed controller	0.377 MW	−0.078 MW	0.455 MW	0.078 MW

- Minimization of power oscillations will be analyzed under R/X grid impedance characteristic.

Acknowledgment

The authors are grateful to Scientific Research Foundation of Van Yuzuncu Yil University (Van, Turkey) for financial support of this study (Project number: FBA-2017-6388).

References

AbdelHady, R. (2017). Modeling and simulation of a micro grid-connected solar PV system. *Water Science*, *31*, 1–10. http://dx.doi.org/10.1016/j.wsj.2017.04.001.

Ali, Z., Christofides, N., Hadjidemetriou, L., et al. (2017). An advanced current controller with reduced complexity and improved performance under abnormal grid conditions. In *PowerTech* (pp. 1–6). http://dx.doi.org/10.1109/PTC.2017.7981082.

Amin, S. M., & Wollenberg, B. F. (2005). Toward a Smart Grid: power delivery for the 21st century. *IEEE Power and Energy Magazine*, *3*(5), 34–41.

Baghaee, H. R., Mirsalim, M., Gharehpetian, G. B., et al. (2017). A decentralized power management and sliding mode control strategy for hybrid AC/DC microgrids

including renewable energy resources. *IEEE Transactions on Industrial Informatics*, 1–10. http://dx.doi.org/10.1109/TII.2017.2677943.

Bai, W., Abedi, M. R., & Lee, K. Y. (2016). Distributed generation system control strategies with PV and fuel cell in microgrid operation. *Control Engineering Practice*, *53*, 184–193. http://dx.doi.org/10.1016/j.conengprac.2016.02.002.

Bayrak, Z. U., Bayrak, G., Ozdemir, M. T., et al. (2016). A low-cost power management system design for residential hydrogen & solar energy based power plants. *International Journal of Hydrocarbon Engineering*, *41*, 12569–12581. http://dx.doi.org/10.1016/j.ijhydene.2016.01.093.

Brka, A., Kothapalli, G., & Al-Abdeli, Y. M. (2015). Predictive power management strategies for stand-alone hydrogen systems: Lab-scale validation. *International Journal of Hydrocarbon Engineering*, *40*, 9907–9916. http://dx.doi.org/10.1016/j.ijhydene.2015.06.081.

Cau, G., Cocco, D., Petrollese, M., et al. (2014). Energy management strategy based on short-term generation scheduling for a renewable microgrid using a hydrogen storage system. *Energy Conversion and Management*, *87*, 820–831. http://dx.doi.org/10.1016/j.enconman.2014.07.078.

Chen, H., Yang, C., Deng, K., et al. (2017). Multi-objective optimization of the hybrid wind/solar/fuel cell distributed generation system using Hammersley Sequence Sampling. *International Journal of Hydrocarbon Engineering*, *42*(12), 7836–7846. http://dx.doi.org/10.1016/j.ijhydene.2017.01.202.

Chilipi, R., Al Sayari, N., Al Hosani, K., et al. (2016). Control scheme for grid-tied distributed generation inverter under unbalanced and distorted utility conditions with power quality ancillary services. *IET Renewable Power Generation*, *10*(2), 140–149. http://dx.doi.org/10.1049/iet-rpg.2015.0095.

Chilipi, R., Al Sayari, N., Al Hosani, K., et al. (2018). Third order sinusoidal integrator (TOSSI)-based control algorithm for shunt active power filter under distorted and unbalanced voltage conditions. *International Journal of Electrical Power & Energy Systems*, *96*, 152–162. http://dx.doi.org/10.1016/j.ijepes.2017.09.026.

Das, V., Padmanaban, S., Venkitusamy, K., et al. (2017). Recent advances and challenges of fuel cell based power system architectures and control–A review. *Renewable and Sustainable Energy Reviews*, *73*, 10–18. http://dx.doi.org/10.1016/j.rser.2017.01.148.

Dash, S. S., Samanta, C., & Ganesan, E. (2016). Modeling, control, and power management for a grid-integrated photo voltaic, fuel cell, and wind hybrid system. *Turkish Journal of Electrical Engineering & Computer Sciences*, *24*, 4804–4823. http://dx.doi.org/10.3906/elk-1404-409.

Divshali, P. H., & Choi, B. J. (2016). Electrical market management considering power system constraints in smart distribution grids. *Energies*, *9*, 1–30. http://dx.doi.org/10.3390/en9060405.

Guo, X., Liu, W., & Lu, Z. (2017). Flexible power regulation and current-limited control of grid-connected inverter under unbalanced grid voltage faults. *IEEE Transactions on Industrial Electronics*, *64*(9), 7425–7432. http://dx.doi.org/10.1109/TIE.2017.2669018.

Guo, X., Wu, W., & Chen, Z. (2011). Multiple-complex coefficient-filter-based phase-locked loop and synchronization technique for three-phase grid-interfaced converters in distributed utility networks. *IEEE Transactions on Industrial Electronics*, *58*, 1194–1204. http://dx.doi.org/10.1109/TIE.2010.2041738.

Jin, P., Li, Y., Li, G., et al. (2017). Optimized hierarchical power oscillations control for distributed generation under unbalanced conditions. *Applied Energy*, *194*, 343–352. http://dx.doi.org/10.1016/j.apenergy.2016.06.075.

Kabiri, R., Holmes, D. G., & McGrath, B. P. (2016). Control of active and reactive power ripple to mitigate unbalanced grid voltages. *IEEE Transactions on Industry Applications*, *52*(2), 1660–1668. http://dx.doi.org/10.1109/TIA.2015.2508425.

Kamali, S. K., Rahim, N. A., & Mokhlis, H. (2014). Smart power management algorithm in microgrid consisting of photovoltaic, diesel, and battery storage plants considering variations in sunlight, temperature, and load. *Energy Conversion and Management*, *84*, 562–582. http://dx.doi.org/10.1016/j.enconman.2014.04.072.

Karimi-Ghartemani, M., & Iravani, M. R. (2002). A nonlinear adaptive filter for online signal analysis in power systems: applications. *IEEE Transactions on Power Delivery*, *17*, 617–622. http://dx.doi.org/10.1109/61.997949.

Karimi-Ghartemani, M., Khajehoddin, S. A., Piya, P., et al. (2016). Universal controller for three-phase inverters in a microgrid. *IEEE Journal of Emerging and Selected Topics in Power Electronics*, *4*(4), 1342–1353. http://dx.doi.org/10.1109/JESTPE.2016.2614956.

Li, J., Wang, Y., Chen, J., et al. (2017). Study on energy management strategy and dynamic modeling for auxiliary power units in range-extended electric vehicles. *Applied Energy*, *194*, 363–375. http://dx.doi.org/10.1016/j.apenergy.2016.09.001.

Liu, H., Hu, H., Chen, H., et al. (2018). Fast and flexible selective harmonic extraction methods based on the generalized discrete Fourier transform. *IEEE Transactions on Power Electronics*, *33*, 3484–3496. http://dx.doi.org/10.1109/TPEL.2017.2703138.

Lopez, M. A. G., De Vicuna, J. L. G., Miret, J., et al. (2018). Control strategy for grid-connected three-phase inverters during voltage sags to meet grid codes and to maximize power delivery capability. *IEEE Transactions on Power Electronics*, 1–15. http://dx.doi.org/10.1109/TPEL.2018.2792478.

Meral, M. E. (2012). Improved phase-locked loop for robust and fast tracking of three phases under unbalanced electric grid conditions. *IET generation, transmission & distribution*, *6*(2), 152–160. http://dx.doi.org/10.1049/iet-gtd.2011.0189.

Meral, M. E., & Çelik, D. (2018a). Benchmarking simulation and theory of various PLLs produce orthogonal signals under abnormal electric grid conditions. *Electrical Engineering*, *100*(3), 1805–1817. http://dx.doi.org/10.1007/s00202-017-0660-x.

Meral, M. E., & Çelik, D. (2018b). Comparison of SRF/PI-and STRF/PR-based power controllers for grid-tied distributed generation systems. *Electrical Engineering*, *100*, 633–643. http://dx.doi.org/10.1007/s00202-017-0530-6.

Meral, M. E., Cuma, M. U., Teke, A., et al. (2014). Experimental and simulation based study of an adaptive filter controlled solid state transfer switch. *Electrical Engineering*, *96*, 385–395. http://dx.doi.org/10.1007/s00202-014-0305-2.

Mirhosseini, M., Pou, J., & Karanayil, B. (2013). Positive-and negative-sequence control of grid-connected photovoltaic systems under unbalanced voltage conditions. In Power engineering conference (pp. 1–6). http://dx.doi.org/10.1109/AUPEC.2013.6725406.

Montanari, A. A., & Gole, A. M. (2017). Enhanced instantaneous power theory for control of grid connected voltage sourced converters under unbalanced conditions. *IEEE Transactions on Power Electronics*, *32*(8), 6652–6660. http://dx.doi.org/10.1109/TPEL.2016.2627049.

Olatomiwa, L., Mekhilef, S., Ismail, M. S., et al. (2016). Energy management strategies in hybrid renewable energy systems: A review. *Renewable and Sustainable Energy Reviews*, *62*, 821–835. http://dx.doi.org/10.1016/j.rser.2016.05.040.

Panda, A. K., & Patnaik, N. (2017). Management of reactive power sharing & power quality improvement with SRF-PAC based UPQC under unbalanced source voltage condition. *Electrical Power and Energy Systems*, *84*, 182–194. http://dx.doi.org/10.1016/j.ijepes.2016.05.010.

Piya, P., Ebrahimi, M., Karimi-Ghartemani, M., et al. (2018). Fault ride-through capability of voltage-controlled inverters. *IEEE Transactions on Industrial Electronics*, *65*(10), 7933–7943. http://dx.doi.org/10.1109/TIE.2018.2803765.

Rashid, M. H. (2014). *Power electronics: Devices, circuits & applications* (4th ed.). Pearson.

Reyes, M., Rodriguez, P., Vazquez, S., et al. (2012). Enhanced decoupled double synchronous reference frame current controller for unbalanced grid-voltage conditions. *IEEE Transactions on power electronics*, *27*(9), 3934–3943. http://dx.doi.org/10.1109/TPEL.2012.2190147.

Rodriguez, P., Pou, J., Bergas, J., et al. (2007). Decoupled double synchronous reference frame PLL for power converters control. *IEEE Transactions on Power Electronics*, *22*(2), 584–592.

Rodriguez, P., Timbus, A., Teodorescu, R., et al. (2007). Flexible active power control of distributed power generation systems during grid faults. *IEEE Transactions on Industrial Electronics*, *54*(5), 2583–2592. http://dx.doi.org/10.1109/TIE.2007.899914.

Saribulut, L., Teke, A., & Tümay, M. (2013). Fundamentals and literature review of Fourier transform in power quality issues. *Journal of Electrical and Electronics Engineering Research*, *5*(1), 9–22. http://dx.doi.org/10.5897/JEEER2013.0436.

Smaoui, M., & Krichen, L. (2016). Control, energy management and performance evaluation of desalination unit based renewable energies using a graphical user interface. *Energy*, *114*, 1187–1206. http://dx.doi.org/10.1016/j.energy.2016.08.051.

Sosa, J. L., Castilla, M., Miret, J., et al. (2016). Control strategy to maximize the power capability of PV three-phase inverters during voltage sags. *IEEE Transactions on Power Electronics*, *31*(4), 3314–3323. http://dx.doi.org/10.1109/TPEL.2015.2451674.

Sun, L. X., Chen, Y., Wang, Z., et al. (2016). Optimal control strategy of voltage source converter-based high-voltage direct current under unbalanced grid voltage conditions. *IET Generation, Transmission & Distribution*, *10*(2), 444–451. http://dx.doi.org/10.1049/iet-gtd.2015.0749.

Sun, L., Wu, G., Xue, Y., et al. (2018). Coordinated control strategies for fuel cell power plant in a microgrid. *IEEE Transactions on Energy Conversion*, *33*(1), 1–9. http://dx.doi.org/10.1109/TEC.2017.2729881.

Wang, F., Duarte, J. L., & Hendrix, M. A. M. (2010). Design and analysis of active power control strategies for distributed generation inverters under unbalanced grid faults. *IET generation, transmission & distribution*, *4*(8), 905–916. http://dx.doi.org/10.1049/iet-gtd.2009.0607.

Wang, F., Duarte, J. L., & Hendrix, M. A. (2011). Pliant active and reactive power control for grid-interactive converters under unbalanced voltage dips. *IEEE Transactions on Power Electronics*, *26*(5), 1511–1521. http://dx.doi.org/10.1109/TPEL.2010.2052289.

Wu, X., Hu, X., Teng, Y., et al. (2017). Optimal integration of a hybrid solar-battery power source into smart home nanogrid with plug-in electric vehicle. *Journal of Power Sources*, *363*, 277–283. http://dx.doi.org/10.1016/j.jpowsour.2017.07.086.

Yang, Y., Blaabjerg, F., Wang, H., et al. (2016). Power control flexibilities for grid-connected multi-functional photovoltaic inverters. *IET Renewable Power Generation*, *10*(4), 504–513. http://dx.doi.org/10.1049/iet-rpg.2015.0133.

Yumurtaci, R. (2013). Role of energy management in hybrid renewable energy systems: case study-based analysis considering varying seasonal conditions. *Turkish Journal of Electrical Engineering & Computer Sciences*, *21*, 1077–1091. http://dx.doi.org/10.3906/elk-1112-85.

Zaibia, M., Champenoisa, G., Roboamc, X., et al. (2018). Smart power management of a hybrid photovoltaic/wind stand-alone system coupling battery storage and hydraulic network. *Mathematics and Computers in Simulation*, *46*, 1–22. http://dx.doi.org/10.1016/j.matcom.2016.08.009.

Zhang, W., Rocabert, J., Candela, J. I., et al. (2017). Synchronous power control of grid-connected power converters under asymmetrical grid fault. *Energies*, *10*(7), 1–21. http://dx.doi.org/10.3390/en10070950.

Zheng, T., Laijun, C. H. E. N., Yan, G. U. O., et al. (2018). Flexible unbalanced control with peak current limitation for virtual synchronous generator under voltage sags. *Journal of Modern Power Systems and Clean Energy*, *6*(1), 61–72. http://dx.doi.org/10.1007/s40565-017-0295-y.